Metallodielectric photonic crystal superlattices: Influence of periodic defects on transmission properties

T. Zentgraf, A. Christ, and J. Kuhl
Max Planck Institute for Solid State Research, 70569 Stuttgart, Germany

N. A. Gippius and S. G. Tikhodeev
A. M. Prokhorov General Physics Institute RAS, Moscow 119991, Russia

D. Nau and H. Giessen
4th Physics Institute, University of Stuttgart, 70550 Stuttgart, Germany
(Received 7 November 2005; published 8 March 2006)

We experimentally and theoretically investigate the influence of periodic defects on the transmission properties of one-dimensional metallodielectric photonic crystal slabs. The spectral positions and the excitation efficiencies of the quasiguided waveguide modes in the slab are determined by the reciprocal lattice vector and the structure factor of the supercells, respectively. We show that by introducing periodic defects in the wire position, the structure factor of the supercells can be strongly modified. For a polarization of the light perpendicular to the wires, the coupling of higher order Bragg resonances of the lattice structure to localized nanowire plasmon resonances can be sensitively controlled by the structure of the supercell. All experimental results show a good agreement with the theory.

DOI: 10.1103/PhysRevB.73.115103 PACS number(s): 78.67.−n, 42.70.Qs, 73.20.Mf

I. INTRODUCTION

Since the proposals by Yablonovitch[1] and John,[2] structures with periodically modulated dielectric permittivity yielding Bragg diffraction of light have attracted not only fundamental but also technological interest. Besides singly periodic crystals, also more complex geometries, such as quasiperiodic structures with two or more incommensurate periods, have been investigated.[3–5] In addition to work on planar structures with asymmetric unit cells[6,7] or artificial disorder,[8,9] especially, doubly periodic structures have been studied extensively.[10] Such structures are composed of conventional slab waveguides which are modified by adding two gratings with different periods. It has been suggested that doubly periodic structures might be able to increase the angular tolerance of resonant grating filters without modifying the spectral bandwidth.[11]

Further effort has been devoted to the analysis of periodic structures with a structured elementary supercell. Such superlattice geometries have been applied in a wide variety of different physical fields, and many interesting fundamental effects have been demonstrated.[12,13] In the optical regime, for example, dielectric superlattice structures support photonic Bloch oscillations.[14] Also, extended wavelength tunability of distributed feedback lasers with a superstructure grating has been demonstrated.[15] Undesired superlattice structures can occur in the fabrication process of photonic crystals. If electron beam lithography is used and larger areas are obtained by stitching of the limited writing field, the error in the positioning will be periodically reproduced and can lead to a superstructure effect in the periodic arrangement.[16]

If the considered periodic structure supports optically active internal excitations such as excitons in quantum nanostructures or particle plasmons in metal nanodots or nanowires, additional coupling effects can appear. A large amount of experimental and theoretical work has been performed to investigate the propagation of collective excitations in these artificial structures.[17] Such optically active photonic crystal structures have recently attracted growing interest, and some fundamental physical effects were demonstrated.[18–21]

In this paper, we present experimental and theoretical studies of metallic photonic crystal superlattice slabs. Such slabs consist of metal nanowire supercells that are periodically deposited on top of a dielectric waveguide slab. We show that the specific superlattice geometry leads to a strong modification of the plasmon resonance in this kind of polaritonic photonic crystal. The modification of the band structure gives rise to coupling phenomena between higher-order Bragg resonances and the localized plasmons in the metal nanowires. We show that the superperiod of the lattice determines the spectral positions of the occurring quasiguided modes, whereas the specific supercell geometry affects the excitation efficiencies. The analysis is based upon optical transmission measurements as well as numerical simulations using a scattering-matrix formalism.[22]

II. SAMPLES AND EXPERIMENTAL TECHNIQUES

Electron beam lithography was used to prepare gold nanowire arrays with a size of 100×100 μm^2 on top of dielectric indium-tin-oxide (ITO) waveguide layers deposited on a quartz substrate. Such a one-dimensional (1D) active photonic crystal structure supports electronic resonances in the form of localized plasmons of the gold nanowires as well as photonic resonances in the form of quasiguided modes of the dielectric ITO layer.[23,24] For all experiments, the ITO layer thickness of 140 nm, the gold nanowire height of 20 nm, and the wire width of 100 nm were kept fixed.

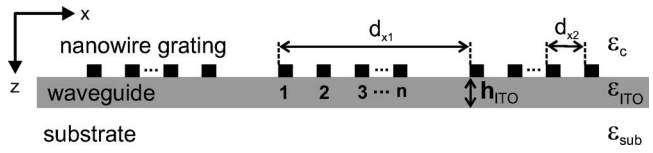

FIG. 1. Schematic view of the sample geometry. The gold nanowires are deposited on top of a dielectric slab waveguide made of ITO. The superperiod is marked by d_{x1} and the subcell period by d_{x2}. For some experiments, the number of nanowires n in the supercell was changed.

A schematic view of the sample structure is shown in Fig. 1. In contrast to a simple grating structure[23,24] with a single wire per unit cell (with period d_{x2}), the superlattice unit cell (supercell) is now composed of a set of n wires by means of adding a specific number of defects (removal or displacement of individual wires). We would like to emphasize that this structure is singly periodic with a superperiod d_{x1}, whereas the periodicity within the supercell (subcell period d_{x2}) is destroyed by inserting defects. However, the degree to which it is destroyed can be effectively controlled by the relative strengths of the inserted defects.

The optical properties of the samples were determined by a standard white-light transmission setup at normal light incidence. In this geometry, the periodic arrangement of the nanowires acts as a surface corrugation, which can be used to excite quasiguided slab modes. In the transverse electric (TE) case where the polarization of the electric field is parallel to the wires, these modes are characterized by sharp spectral features in the extinction spectrum. In transverse magnetic (TM) polarization, the light field can excite an additional collective oscillation of the conduction band electrons in the gold nanowires. This spectrally broad resonance, a so-called particle plasmon, can couple to the quasiguided modes of the slab to form a waveguide-plasmon polariton.[23]

III. EXPERIMENTAL AND THEORETICAL RESULTS

In this work, three different sample series for polarization directions parallel (TE) and perpendicular (TM) to the wires will be investigated to demonstrate the influence of various superlattice configurations on the optical transmission spectra (the plane of light incidence was kept perpendicular to the wires, i.e., x-z plane in Fig. 1). We will show that the supercell geometry determines the excitation efficiencies of the possible waveguide modes.

In the first superlattice design *A*, only the number of nanowires per supercell was changed while all other parameters were kept fixed. In the second design *B*, the superperiod of the lattice was varied by means of expanding the distance between the supercells. In the third design *C*, periodic defects in the wire positions in each supercell were introduced with controlled magnitude. All experimental results are compared with calculations using a scattering matrix formalism and Fourier decomposition of the grating structure.

A. Influence of the supercell structure

For the first sample series, we start with a singly periodic structure with a fixed period of $d_x = d_{x2} = 440$ nm. This perfect grating structure can be interpreted as a superlattice in some respects. Introducing, e.g., a superperiod of 6×440 nm $= 2640$ nm, the structure exhibits six nanowires within each individual supercell. Now the number of wires per supercell [with a fixed superperiod $d_{x1} = 2640$ nm, see Fig. 2(a)] is decreased one by one, so that we end up in a simple lattice with a single wire per supercell.

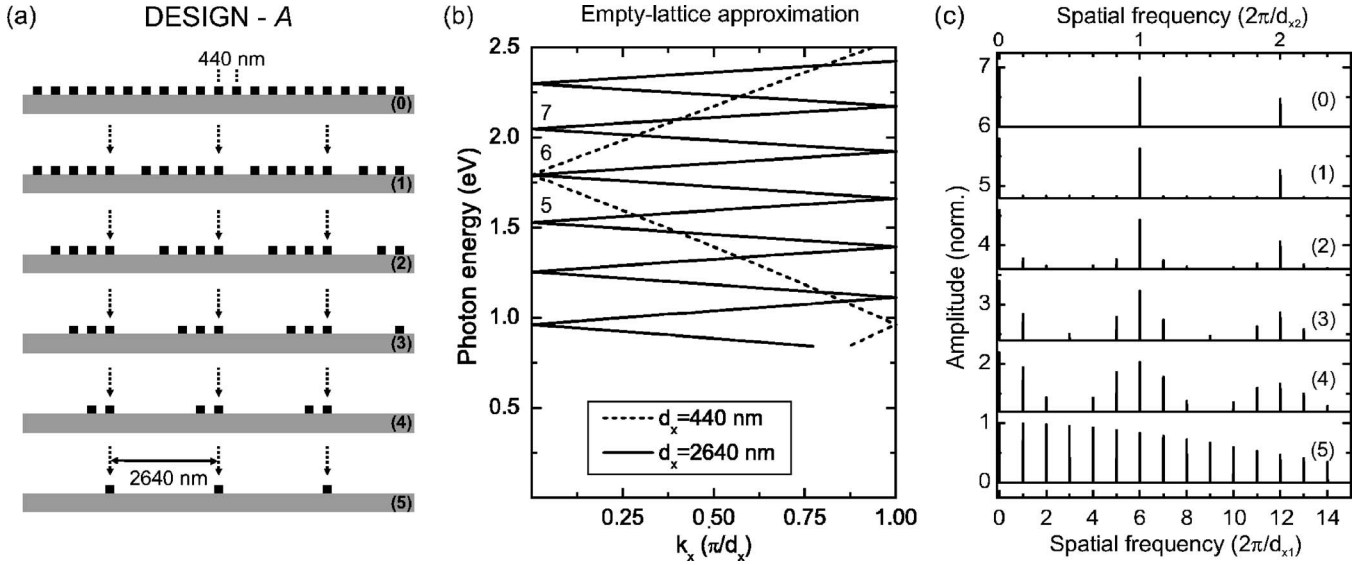

FIG. 2. (a) Schematic views of the sample geometries for design *A*. While the superperiod $d_{x1} = 2640$ nm and the subcell period $d_{x2} = 440$ nm have been retained unchanged in this series, the number of missing nanowires per supercell is increased stepwise from 0 to 5. Dispersion relations of TE guided modes obtained by the empty-lattice approximation are shown in (b). The modes are folded into the first Brillouin zone of a lattice with periods $d_x = 440$ nm (dotted line) and $d_x = 2640$ nm (solid line). The numbers indicate the order of the Bragg resonance at the zone center for the period of $d_x = 2640$ nm. In (c) the Fourier decompositions of the grating structures are presented in dependence on the spatial frequency. The number in brackets denotes the sample in this series.

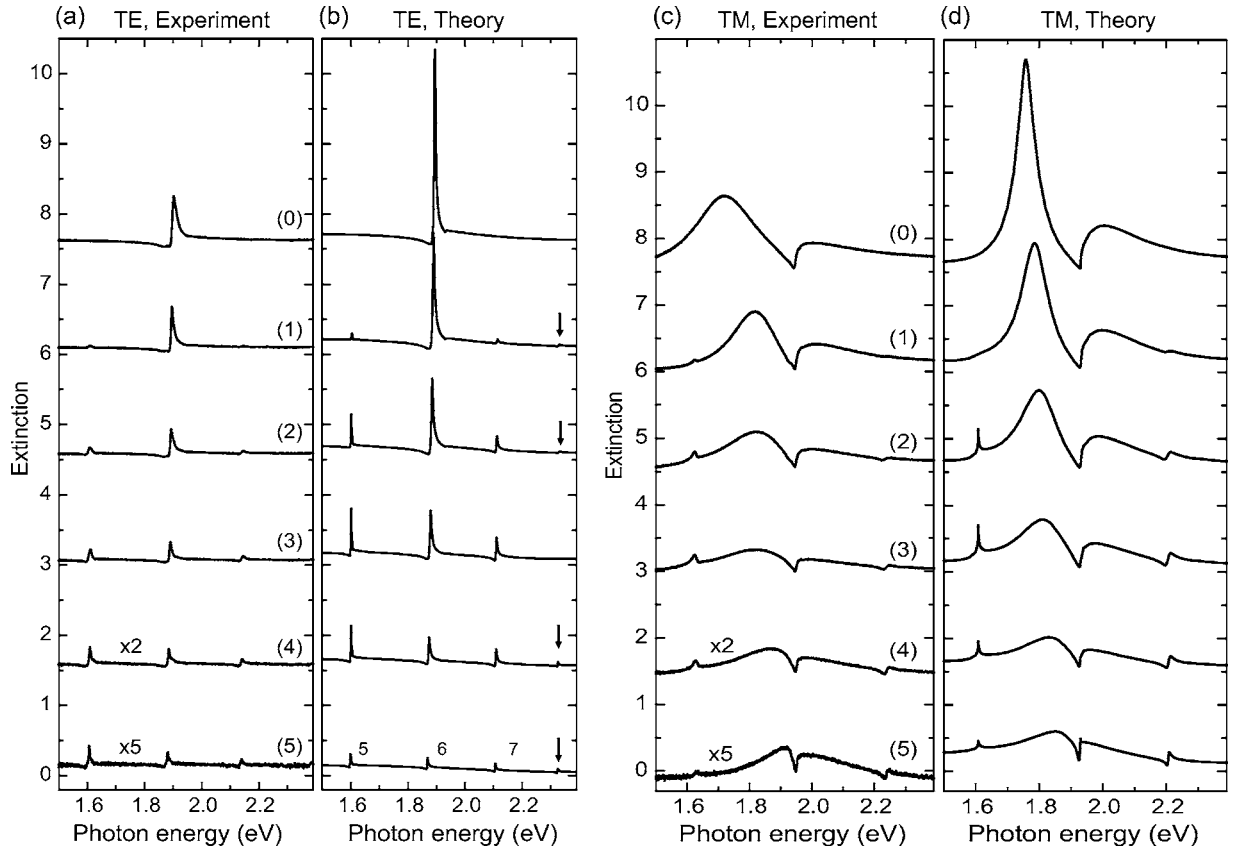

FIG. 3. Measured (a), (c) and calculated (b), (d) extinction spectra of the sample design *A* of metallodielectric superlattice structures for normal light incidence and both polarization directions. The number in brackets denotes the sample in this series. The individual spectra are shifted upward for clarity in each panel. While the periods $d_{x1}=2640$ nm and $d_{x2}=440$ nm have been retained unchanged, the number of missing nanowires per supercell is increased stepwise from 0 to 5. The arrows mark the eighth Bragg resonance. For better visibility of the peaks, the experimentally obtained spectra (4) and (5) in panels (a) and (c) are multiplied by a factor of 2 and 5, respectively.

The experimental results for this structure design and TE polarization are shown in Fig. 3(a). The extinction spectra are characterized by various sharp spectral features, which can be related to the excitation of quasiguided modes in the ITO waveguide of the photonic crystal slab structure. All experimental spectra in Fig. 3(a) are well reproduced by scattering-matrix-based calculations.[22] The obtained theoretical results for TE polarization are depicted in Fig. 3(b). The measured linewidths of the individual modes in TE polarization deviate slightly from the theoretical values. Although the observed broadening can be partially explained by fabrication tolerances (e.g., variation of the exact periods) and surface roughness, especially the limited number of illuminated supercells ($\approx$20) due to finite beam diameter in the experiment has to be taken into account. The fabrication tolerances are also important for the plasmon resonances in TM polarization. They lead to a faster decay (homogeneous broadening) and a distribution (inhomogeneous broadening) of the plasmon resonances. For convergence of the truncated scattering matrix, we used 301 harmonics for TE and 451 harmonics for TM polarization.

As expected for the structure with the perfect periodicity of 440 nm, the uppermost extinction spectra (denoted as "0") are characterized by a single resonance peak at $\approx$1.9 eV within the shown spectral range. This peak can be simply explained by the excitation of the symmetric band-edge eigenstate at the second-order stopband. An empty-lattice approximation can help to understand the position of the resonance in the spectrum. In this approximation, a rough estimate of the spectral position of the mode can be obtained assuming a homogeneous waveguide by folding the dispersion relation of the TE mode back into the first Brillouin zone of the periodically corrugated waveguide structure [dotted line in Fig. 2(b)].

In Figs. 3(a) and 3(b), additional peaks immediately arise below and above this single extinction maximum, when the number of nanowires is decreased stepwise and defects (missing nanowires) are introduced periodically. The spectral positions of the resonances are almost independent of the number of wires per supercell. A remaining slight shift is caused by a change of the effective refractive index of the waveguide slab due to the removed gold wires. While the extinction of the central peak at $\approx$1.9 eV is constantly reduced, the appearing additional resonances show a rather complex behavior. Finally, the lowermost spectra (5) are characterized by a couple of extinction maxima which are more or less evenly distributed and weakly pronounced.

Again the empty-lattice approximation can be used to clarify the origin of the appearing additional resonances. The zone-folding demonstrates that the spectral position of the individual resonances is unambiguously determined by the

superperiod $d_{x1}=2640$ nm. As shown in Fig. 2(b), the folding of the TE mode of the homogeneous waveguide results in a strongly modified band diagram for this corrugation period. Now the higher order Bragg resonances at the zone center are lowered in energy due to a size reduction of the Brillouin zone by the larger period of 2640 nm (solid line). According to the empty-lattice approximation, the observed resonant features of the superlattice structure can be related to higher order Bragg resonances. Therefore, the lowest peak in the spectra at ≈ 1.6 eV in Fig. 3(a) corresponds to the fifth Bragg resonance. The strongest extinction peak at ≈ 1.9 eV for example can be interpreted as the sixth Bragg resonance at the zone center of the photonic crystal band structure with a period of 2640 nm. Due to the specific geometry, the spectral position of the sixth Bragg resonance in the superlattice framework corresponds to the first Bragg resonance of a lattice with a regular period of 440 nm.

Although the simple empty-lattice picture can be used to calculate the approximate positions of the peaks in the superlattice structure, the model makes no predictions about the excitation efficiencies of the individual modes. However, more information concerning the efficiencies can be obtained by Fourier decomposition of the grating geometry. Yariv and Nakamura showed, in a detailed analysis of periodically corrugated waveguides, that in the theory of mode coupling in planar photonic crystal structures, the coupling strength is brought about by the amplitudes of the corresponding Fourier harmonics of the spatial lattice.[25]

Strictly speaking, such coupled-mode analysis is valid only in the weak coupling regime, which corresponds to a small waveguide corrugation. Although our case is more complicated, these arguments still work qualitatively, as can be seen from the comparison between the scattering-matrix calculations and the simple Fourier analysis. According to the latter, the coupling strength between the incoming wave at normal incidence and the pair of counter-propagating TE modes with momenta $G_l=\pm 2\pi l/d_x$ $(l=1,2,\ldots)$ is proportional to the amplitude of the lth Fourier harmonic of the spatial perturbation. Then the power P_l flowing from the incident light into the quasiguided mode with momentum G_l is proportional to the squared modulus of the amplitude of the lth Fourier harmonic

$$P_l \sim |F(\mathbf{G}_l)|^2 = \left| \int F(\mathbf{r}) \cdot \exp(-\mathrm{i}\mathbf{G}_l \cdot \mathbf{r}) d^3r \right|^2, \qquad (1)$$

where $F(\mathbf{r})$ is the spatial scattering potential of the lattice structure.

The results are analogous to the technique of structure determination of solids from x-ray diffraction experiments,[26] where in a kinematic approximation of elastic scattering, the intensity of the scattered beam is proportional to the square of the structure factor (i.e., the Fourier transform) of the crystal unit cell.

For a quantitative prediction of the excitation efficiencies, the specific nanowire arrangement has been modeled using Eq. (1). In our approximation, we substituted $F(\mathbf{r})$ with the 1D lattice geometry of the sample. As spatial resolution, we used a discretization of 1 nm. The scattering potential at each point of the nanowires was set to one, while all other values were zero. The squared modulus of the individual Fourier components in dependence on the spatial frequency of the superlattice structure is shown in Fig. 2(c). Due to the mirror symmetry of the grating structure, only the positive spatial harmonics are depicted. As expected, the Fourier decomposition of the two perfect grating structures, (0) and (5), results in regular distribution in reciprocal space too, where only the amplitudes for multiples of the reciprocal lattice vector are nonzero. Also the amplitudes of higher spatial frequencies are reduced due to the finite width of the nanowires.

It is important to note that our previously discussed superlattice series is somewhat special. The reciprocal lattice vector $(2\pi/d_{x2})$ of grating structure (0) is a direct multiple of the reciprocal vector $(2\pi/d_{x1})$ of structure (5). Therefore, the first Fourier harmonic of the structure (0) can alternatively be interpreted as the sixth spatial harmonic of a superlattice with a superperiod of $d_{x1}=2640$ nm. If the number of nanowires and, therefore, the structure of the supercell is modified without changing the superperiod, the amplitudes of the spatial harmonics show a quite complex behavior in dependence on the specific supercell geometry. A more precise comparison between Fig. 3(a) and Fig. 2(c) reveals that the excitation efficiencies of the Bragg resonances are directly correlated with the spatial Fourier harmonics of the superlattice. A larger amplitude of a particular spatial harmonic results in a stronger excitation of the corresponding Bragg resonance and, therefore, a larger peak in the extinction spectrum. Due to the fact that only normalized amplitudes are displayed in Fig. 2(c), the specific intensity distributions of the extinction maxima have to be interpreted with respect to the amplitude of the sixth Bragg resonance in the Fourier spectrum.

Even small details of the extinction spectra can be found in the related Fourier decompositions. The eighth Bragg resonance of the TE mode (marked by arrows in Fig. 3) for example is suppressed in the spectrum of the superlattice structure (3). This observation is clearly confirmed by the corresponding Fourier decomposition of structure (3), where the amplitude of the eighth spatial harmonic is zero. An analogous situation can be observed in x-ray diffraction where certain diffraction orders are missing in some special crystal classes although the appropriate Bragg condition is satisfied, i.e., the structure factor is equal to zero.

For TM polarization and normal light incidence, the measured extinction spectra look quite different in comparison to the TE case [Fig. 3(c)]. Now the electric field is oriented perpendicular to the gold nanowires and can excite the nanowire plasmon resonance.[23] In contrast to TE polarization, the TM polarized spectrum (0) of Fig. 3 exhibits two extinction maxima in the considered spectral range. Due to the strong coupling between the TM quasiguided modes and the localized particle plasmons, one can observe a spectral mode splitting instead of a spectral overlap of the resonances.[24] Therefore, the splitting of the plasmon resonance can be interpreted as the formation of a new polaritonic state, similar to the normal mode coupling in semiconductor microcavities.[27]

Removing individual nanowires of the supercell leads to the excitation of higher order Bragg resonances of the super-

period analogous to the quasiguided modes in TE polarization. Due to the larger period d_{x1} of the superlattice, the energetic gap between the modes is smaller than for a simple lattice with a period of d_{x2} (see TE polarization). Therefore, more than one higher order Bragg resonance of the TM mode can couple to the plasmon resonance of the nanowires. As can be seen in Fig. 3(c), the normal mode splitting decreases with the number of missing wires. In the polariton picture, this behavior is an indication of reduced coupling strength between the two resonances due to the lower excitation efficiency of the higher order waveguide modes.[28]

This sample series demonstrates that the structure of the supercell in the superlattice geometry influences the excitation efficiency of the modes and, therefore, the coupling to the plasmon resonance.

B. Influence of the superperiod

The specific influence of the superperiod d_{x1} is demonstrated by a second sample series (design *B*). The schematic view of the considered sample structures is displayed in Fig. 4(a). All sample structures are again based on gold nanowire arrays deposited on top of a 140-nm-thick ITO waveguide layer. While the subcell period of 475 nm and the number of nanowires ($n=10$) per supercell have been kept constant for all samples in this series, only the superperiod d_{x1} is increased from 4750 nm (0) to 5550 nm (8) in steps of 100 nm. Apart from structure (0), the superperiod d_{x1} is no longer an exact multiple of the subcell period d_{x2}. The experimental and theoretical extinction spectra for this series are shown in Fig. 5. The qualitative agreement is excellent and only small deviations are observable. In comparison to the experimentally detected resonances, the corresponding theoretical peaks obtained by the scattering matrix method are slightly blueshifted. This fact can be related to uncertainties in the exact determination of the nanowire periods. For the deviation of the linewidths, the same arguments used in the discussion of design *A* hold.

The emerging extinction maxima in TE polarization show a rather complex behavior depending on the superperiod d_{x1}. In contrast to the results of Fig. 3, the excitation efficiencies as well as the spectral positions of the TE modes are now strongly influenced by changing the superperiod. All observed extinction maxima are caused by the excitation of higher order Bragg resonances. The three resonant features of structure (8), for example, can be attributed to the 10th, 11th, and 12th Bragg resonance of the TE mode at the zone center of the Brillouin zone. Generally, all superlattice spectra, except for structure (0), are characterized by at least two more or less pronounced maxima in the considered spectral range, while all others are suppressed simultaneously. The relative amplitudes of the extinction maxima are again well described by the amplitudes of the corresponding Fourier decomposition of the spatial structure [Fig. 4(b)].

Superlattice design *B* clearly confirms the intuitive model for the excited modes. While the superperiod d_{x1} determines the spectral positions of the supported modes (higher order Bragg resonances), their individual excitation efficiencies, on the other hand, are directly related to the specific subcell

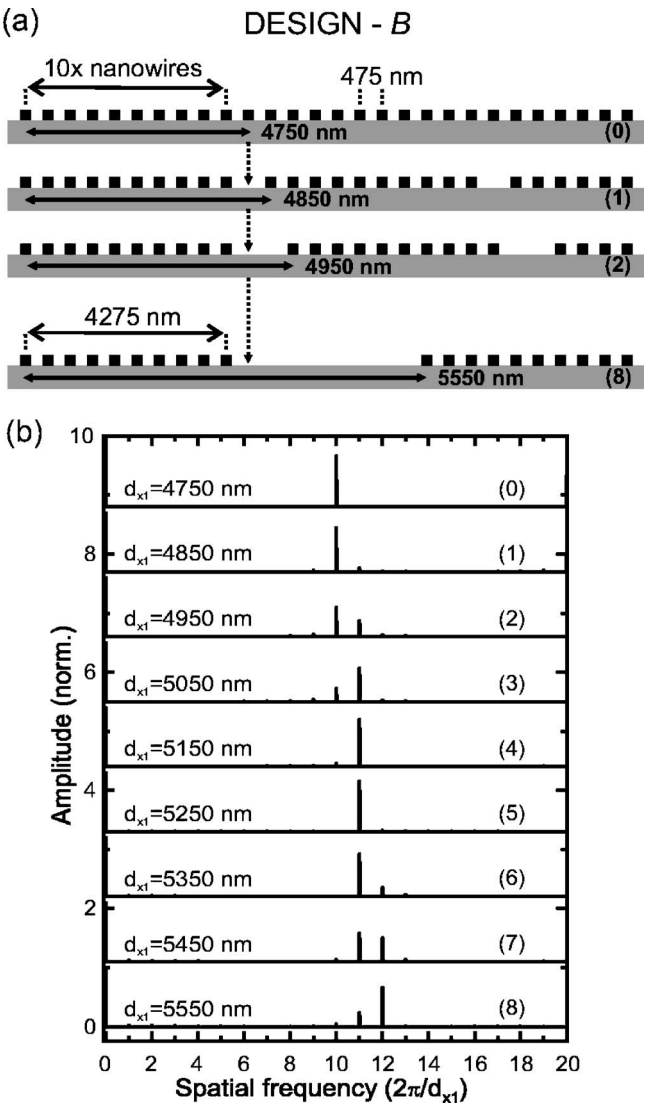

FIG. 4. (a) Schematic views of the sample geometries for design *B*. The number in brackets denotes the sample in this series. While the subcell period $d_{x2}=475$ nm and the number of nanowires ($n=10$) have been kept constant for all samples in this series, the superperiod d_{x1} is increased from 4750 nm (0) to 5550 nm (8) in steps of 100 nm. In (b), the Fourier decompositions of the grating structures are shown in dependence on the spatial frequency and the superperiod d_{x1}.

period d_{x2}. The stepwise reduction of the size of the Brillouin zone, i.e., an increased superlattice period, leads to a reduction of the resonance energies of the individual Bragg resonances. The 11th Bragg resonance, for example [see Fig. 5(b)], is shifted from 1.87 eV in structure (1) to approximately 1.66 eV in structure (8). Simultaneously, the extinction efficiencies are also strongly modulated. After a first enhancement (increased extinction), the mode is again attenuated for larger periods. Generally, the *l*th Bragg resonance reaches its extinction maximum when the *l*th multiple of the reciprocal lattice vector $2\pi/d_{x1}$ coincides with the reciprocal lattice vector $2\pi/d_{x2}$ of the subcell. This important fact is clearly visible in the measured and calculated extinction spectra. Only those higher order Bragg resonances

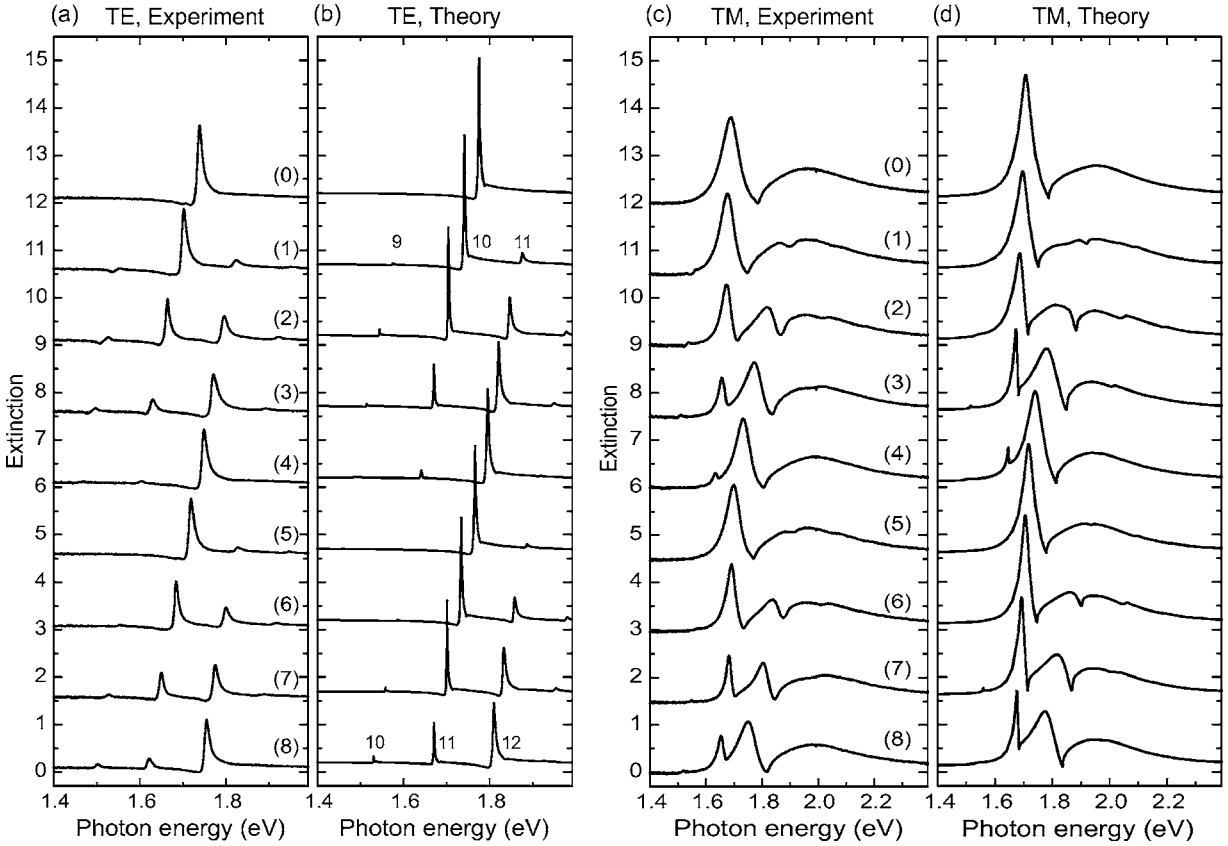

FIG. 5. Measured (a), (c) and calculated (b), (d) extinction spectra of the sample design *B* of metallodielectric superlattice structures for normal light incidence and both polarization directions. The individual spectra are shifted upward for clarity in each panel. Again, the number in brackets denotes the sample. While the subcell period of 475 nm and the number of nanowires ($n=10$) per supercell have been kept constant for all samples with this design, the superperiod d_{x1} is increased from 4750 nm (0) to 5550 nm (8) in steps of 100 nm. The numbers in panel (b) denote the order of the Bragg resonances.

whose spectral positions are close to the first Bragg resonance of a regular grating with exact period of 475 nm show up in the obtained spectra. It is the structure factor, i.e., the Fourier transform of the supercell spatial structure, which determines the amplitudes of the individual peaks.

For TM polarization and normal light incidence, the plasmon resonance is again visible in the extinction spectra [Figs. 5(c) and 5(d)]. Similar to design *A*, the plasmon resonance shows the typical polariton behavior for the singly periodic structure (0). When increasing the superperiod, additional dips in the plasmon resonance appear. Again the higher order Bragg resonances for TM polarization can couple to the plasmon and form waveguide-plasmon polaritons (1)–(8). In this sample design, the spectral positions of the quasiguided modes are not fixed, but change with the superperiod of the lattice. Therefore, the spectral position of the peaks in the plasmon resonance change with the superperiod due to the coupling effect to the optical waveguide modes. In contrast to periodic structures with a simple unit cell,[24] where only the positions of the quasiguided modes are influenced by the lattice period, in the superlattice design, the excitation efficiencies are additionally determined by the subcell structure. This kind of form shape or structure factor can be used to modify independently the coupling strength to the plasmon resonance and the spectral position of the waveguide modes.

The original extinction spectrum (0) of design *B* is nearly reproduced for a superperiod of $d_{x1}=5250$ nm (5), where d_{x1} is approximately an exact multiple of the subcell period d_{x2}. The experimental results show clearly that the subcell period does not only influence which TM mode will be excited but also the excitation efficiency and therefore the coupling strength to the plasmon resonance. Again all spectra are well reproduced by scattering matrix calculations.

C. Nonperiodic subcells

Using a third sample series (design *C*), we will demonstrate that the subcell period acts as a structure factor of the excitation efficiencies of the higher order modes. From solid state physics, it is well known that the diffraction intensities in x-ray scattering experiments strongly depend on the temperature of the crystal.[29] The thermal movement of the atoms in random directions leads to a variable distance between next neighbors. As a consequence, the peak intensities of the scattered light of the diffraction orders are reduced while the linewidths are preserved.[30]

In the following, we use this physical effect to change the structure factor of the supercells in a fixed superlattice geometry. For modeling the "temperature dependence" in our structures, we used a superlattice similar to structure (1) of design *A* but with six nanowires per supercell (see Fig. 6). In

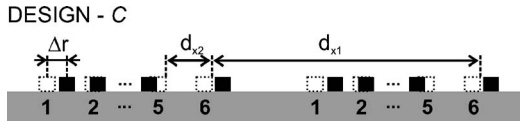

FIG. 6. Schematic view of the sample geometry for design *C*. While all fundamental periods have been kept constant in this series, a small random displacement Δr in the positions of the nanowires was introduced. The dotted squares mark the cross section of original positions of the nanowires without displacement. The individual wires in each supercell are labeled by the numbers 1 to 6. Notice that the same randomization was used in each supercell within the structure, i.e., all wires "1" have the same displacement Δr.

this series, the subcell period $d_{x2}=475$ nm and the number of nanowires have been kept constant. The superperiod $d_{x1}=3325$ nm was chosen as an exact multiple of the subcell period. Hence, only one pronounced waveguide mode appears in the relevant spectral range (see Fig. 7 uppermost spectrum) in analogy to structure (1) of the first sample series. The temperature of the lattice was modeled by introducing periodic defects, i.e., by changing the nanowire positions. The deviations Δr of the individual positions were determined by $\Delta r=fR$ for a weighting factor f and a set of six random distances R of a uniform distribution (−135 nm to 135 nm). The width of the distribution R was limited to avoid crossing of the nanowire positions. A new set of R was used for each weighting factor f. For the scattering matrix simulations, we used the identical displacement (same set of R) in each supercell of the lattice. We notice that this kind of disorder is very special and only a rough approximation of thermal disorder. For example, the spectral distance between the Bragg resonances is fixed because the superperiodicity

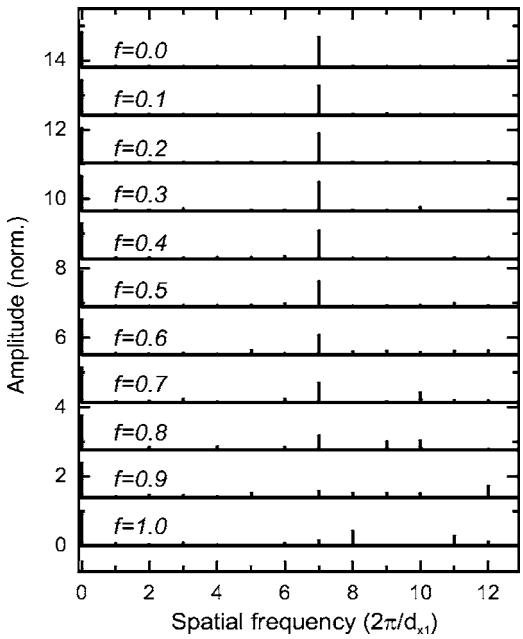

FIG. 7. Fourier decompositions of the grating structures (design *C*) in dependence on the spatial frequency and the strength f of the displacement. The individual Fourier spectra are shifted upward for clarity.

d_{x1} is not destroyed at all. Strictly speaking, only in the case of a very large number of randomly displaced nanowires in the superperiod, $d_{x1}\gg l_c$, where l_c is the coherence length of the photonic modes (either quasiguided in TE or waveguide-plasmon polaritons in TM), this becomes a good model for thermal effects in a perfect lattice with a simple period d_{x2} along the grating.

The experimental and theoretical results for this structure design are shown in Fig. 8. For the first sample without any displacement of the positions ($f=0$), one strong peak is visible in TE polarization. This peak can be attributed to the seventh Bragg resonance at the zone center of the reciprocal lattice vector $2\pi/d_{x1}$. Since the superperiod is an exact multiple (7×475 nm) of the subcell period, only higher order Bragg resonances of the superperiod which are multiples of 7 (7th, 14th, etc.) can be efficiently excited. By diminishing influence of the subcell periodicity d_{x2} with introducing periodic displacements, the selection of distinct waveguide modes can no longer take place. Therefore, the formally suppressed resonances of the superperiod d_{x1} will become more pronounced.

In Fig. 8(a), additional peaks arise below and above the single resonance when the displacement of the wires in the lattice is increased. While the excitation efficiency of the seventh Bragg resonance is reduced, other TE modes appear more pronounced. The subcell periodicity is overwritten by the random displacement and does not act as a structure factor for the superperiod anymore. Due to the very special manner of destroying the structure factor in our samples, the change in the wire positions influences only the subcell periodicity. The superperiod d_{x1} is not influenced in this case.

For TM polarization and normal light incidence, the spectra show a similar behavior as in TE polarization. The additional quasiguided modes couple to the localized particle plasmon resonance and lead to further dips in the extinction spectra. This behavior can be well observed for the weighting factor of $f=1.0$ (strong displacement), where the plasmon resonance shows two clearly pronounced dips. With increasing displacement, the splitting of the polariton at 1.8 eV is reduced due to the weaker excitation efficiency of the seventh Bragg resonance of the superlattice. Simultaneously, the sixth Bragg resonance appears more pronounced because the structure factor of the other higher order resonances is distinct from zero now. Although the displacement of the wires leads to a complex lattice structure, all spectra are again well reproduced by the scattering matrix calculations.

In the case of strong deviations of the periodic wire positions ($f>0.6$), some modes are missing in the measured and calculated optical extinction spectra in Fig. 8. This fact is especially visible in TE polarization. To clarify the origin of the low excitation efficiency of these modes, the structure factor for each sample was calculated by Fourier decomposition of the lattice geometry. The results are shown in Fig. 7. The amplitudes of the spatial harmonics show a complex behavior when increasing the displacement. For a certain strength of displacement, several harmonics vanish and appear again when changing the strength. This behavior is due to the very specific design of our samples. The periodic defects lead to special structure factors of the lattice for each strength of displacements. Theoretical calculations show that

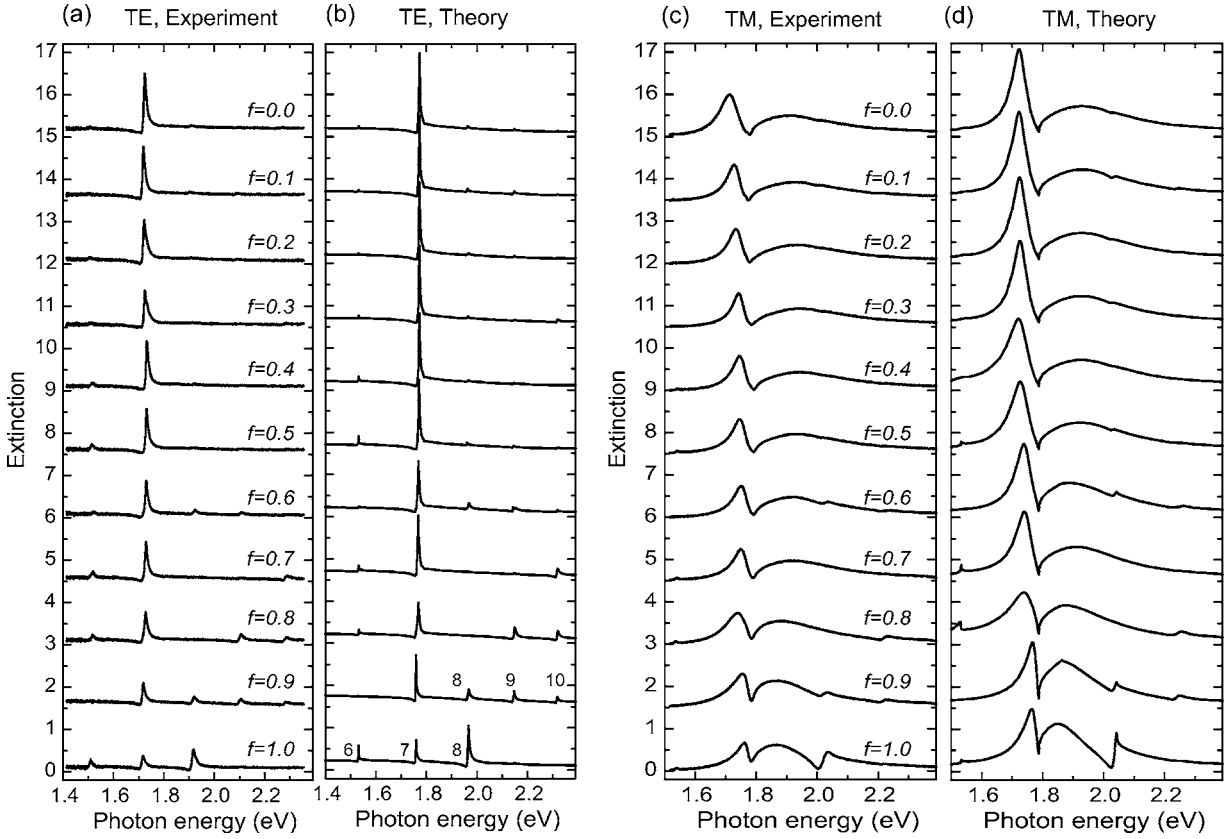

FIG. 8. Measured (a), (c) and calculated (b), (d) extinction spectra of the sample design *C* of metallodielectric superlattice structures for normal light incidence and both polarization directions. The individual spectra are shifted upward for clarity in each panel. While the subcell period of 475 nm, the number of nanowires ($n=6$), and the superperiod of 3325 nm have been kept constant for all samples with this design, periodic defects in the position of the nanowires were introduced from $f=0$ (no defects, $\Delta r_{\max}=0$) to $f=1.0$ ($\Delta r_{\max}=\pm 135$ nm) in steps of 0.1. The numbers in panel (b) denote the order of the Bragg resonance. All extinction values in panel (a) are multiplied by a factor of 2 for better visibility of the peaks.

a change in the wires arrangement (the other set of *R*) but with the same weighting factor for the displacement can lead to completely different excitation efficiencies of the modes. Therefore, depending on the specific wire positions, some modes can vanish and appear again in different samples with the same amount of defects.

IV. CONCLUSION

In conclusion, we have shown that the optical properties of planar metallodielectric photonic crystals can be strongly modified by realizing a superlattice geometry. The influence of the superperiod d_{x1}, the subcell period d_{x2}, and the number of nanowires *n* in the supercell have been analyzed in TE and TM polarization. In the case of TE polarization, only the quasiguided TE modes of the ITO waveguide slab can be excited. The spectra clearly show that the superperiod d_{x1} determines the energy positions of the appearing resonances, whereas the subcell period acts as a structure factor for these modes. Therefore, the excitation efficiency and the energy position of the quasiguided modes can be influenced independently. For TM polarization, strong coupling phenomena have been found. All higher order Bragg resonances, which energetically overlap with the plasmon resonance, can couple to the localized nanowire plasmons and form waveguide-plasmon polaritons. The coupling strength depends on the excitation efficiencies of the quasiguided modes. In the superlattice geometry, narrow dips in the plasmon resonance can, therefore, be created. When introducing periodic defects in the nanowire positions, the influence of the structure factor of the subcell is reduced and other higher order Bragg resonances can be excited. All experimental observations were well reproduced by calculations with a scattering matrix method and qualitatively explained by Fourier decomposition of the lattice structure.

ACKNOWLEDGMENTS

This work was financially supported by the German Federal Ministry of Education and Research (Grant No. FKZ 13N8340/1), the Deutsche Forschungsgemeinschaft (Priority Program Grant Nos. SPP1113 and FOR557), Russian Academy of Sciences (Program "Low-dimensional quantum structures," 2.3), and Russian Foundation for Basic Research (Grant No. 03-02-17314). The authors thank K. von Klitzing for continuous support.

[1] E. Yablonovitch, Phys. Rev. Lett. **58**, 2059 (1987).
[2] S. John, Phys. Rev. Lett. **58**, 2486 (1987).
[3] M. Kohmoto, B. Sutherland, and K. Iguchi, Phys. Rev. Lett. **58**, 2436 (1987).
[4] P. L. Gourley, C. P. Tigges, J. R. P. Schneider, T. M. Brennan, B. E. Hammons, and A. E. McDonald, Appl. Phys. Lett. **62**, 1736 (1993).
[5] S. D. Gupta and D. S. Ray, Phys. Rev. B **41**, 8047 (1990).
[6] T. Fujita, T. Kitabayashi, A. Seki, M. Hirasawa, and T. Ishihara, Physica E (Amsterdam) **7**, 681 (2000).
[7] N. A. Gippius, S. G. Tikhodeev, and T. Ishihara, Phys. Rev. B **72**, 045138 (2005).
[8] V. Yannopapas, A. Modinos, and N. Stefanou, Opt. Quantum Electron. **34**, 227 (2002).
[9] D. Nau, A. Christ, S. Linden, J. Kuhl, and H. Giessen, *CLEO/IQEC and PhAST Technical Digest on CD-ROM* (OSA, Washington, DC, 2004), p. IThB6.
[10] S. T. Peng, J. Opt. Soc. Am. A **7**, 1448 (1990).
[11] F. Lemarchand, A. Sentenac, and H. Giovannini, Opt. Lett. **23**, 1149 (1998).
[12] S. Ivanov, A. Toropov, S. Sorokin, T. Shubina, A. Lebedev, P. Kop'ev, Z. Alferov, H. J. Lugauer, G. Reuscher, M. Keim, F. Fischer, A. Waag, and G. Landwehr, Appl. Phys. Lett. **73**, 2104 (1998).
[13] W. Park and C. J. Summers, Appl. Phys. Lett. **84**, 2013 (2004).
[14] R. Sapienza, P. Costantino, D. Wiersma, M. Ghulinyan, C. J. Oton, and L. Pavesi, Phys. Rev. Lett. **91**, 263902 (2003).
[15] V. Jayaraman, Z. M. Chuang, and L. A. Coldren, IEEE J. Quantum Electron. **29**, 1824 (1993).
[16] Y. Sheng, Y. Qui, and J. Wang, Opt. Eng. (Bellingham) **43**, 2570 (2004).
[17] E. L. Albuquerque and M. G. Cottam, Phys. Rep. **233**, 67 (1993).
[18] S. Nojima, Phys. Rev. B **61**, 9940 (2000).
[19] E. L. Ivchenko, M. M. Voronov, M. V. Erementchouk, L. I. Deych, and A. A. Lisyansky, Phys. Rev. B **70**, 195106 (2004).
[20] S. Linden, J. Kuhl, and H. Giessen, Phys. Rev. Lett. **86**, 4688 (2001).
[21] T. Zentgraf, A. Christ, J. Kuhl, and H. Giessen, Phys. Rev. Lett. **93**, 243901 (2004).
[22] S. G. Tikhodeev, A. L. Yablonskii, E. A. Muljarov, N. A. Gippius, and T. Ishihara, Phys. Rev. B **66**, 045102 (2002).
[23] A. Christ, S. G. Tikhodeev, N. A. Gippius, J. Kuhl, and H. Giessen, Phys. Rev. Lett. **91**, 183901 (2003).
[24] A. Christ, T. Zentgraf, J. Kuhl, S. G. Tikhodeev, N. A. Gippius, and H. Giessen, Phys. Rev. B **70**, 125113 (2004).
[25] A. Yariv and M. Nakamura, IEEE J. Quantum Electron. **13**, 233 (1977).
[26] W. Friedrich, P. Knipping, and M. Laue, Ann. Phys. **41**, 971 (1913).
[27] C. Weisbuch, M. Nishioka, A. Ishikawa, and Y. Arakawa, Phys. Rev. Lett. **69**, 3314 (1992).
[28] T. Zentgraf (unpublished).
[29] I. Waller and R. W. James, Proc. R. Soc. London **117**, 214 (1927).
[30] C. Kittel, *Introduction to Solid State Physics*, 8th ed. (Wiley, New York, 2005).